ARMY RESEARCH LABORATORY

Measurement of the Two-photon Absorption Coefficient of Gallium Phosphide (GaP) Using a Dispersion-minimized Sub-10 Femtosecond Z-scan Measurement System

by Robert C. Hoffman and Andrew G. Mott

ARL-TR-6157 **September 2012**

NOTICES

Disclaimers

The findings in this report are not to be construed as an official Department of the Army position unless so designated by other authorized documents.

Citation of manufacturer's or trade names does not constitute an official endorsement or approval of the use thereof.

Destroy this report when it is no longer needed. Do not return it to the originator.

Army Research Laboratory
Adelphi, MD 20783-1197

ARL-TR-6157 **September 2012**

Measurement of the Two-photon Absorption Coefficient of Gallium Phosphide (GaP) Using a Dispersion-minimized Sub-10 Femtosecond Z-scan Measurement System

Robert C. Hoffman and Andrew G. Mott
Sensors and Electron Devices Directorate, ARL

REPORT DOCUMENTATION PAGE

Form Approved
OMB No. 0704-0188

1. REPORT DATE *(DD-MM-YYYY)*	2. REPORT TYPE	3. DATES COVERED (From - To)
September 2012	Final	August 2012

4. TITLE AND SUBTITLE
Measurement of the Two-photon Absorption Coefficient of Gallium Phosphide (GaP) Using a Dispersion-minimized Sub-10 Femtosecond Z-scan Measurement System

5a. CONTRACT NUMBER

5b. GRANT NUMBER

5c. PROGRAM ELEMENT NUMBER

6. AUTHOR(S)
Robert C. Hoffman and Andrew G. Mott

5d. PROJECT NUMBER

5e. TASK NUMBER

5f. WORK UNIT NUMBER

7. PERFORMING ORGANIZATION NAME(S) AND ADDRESS(ES)
U.S. Army Research Laboratory
ATTN: RDRL-SEE-M
2800 Powder Mill Road
Adelphi, MD 20783-1197

8. PERFORMING ORGANIZATION REPORT NUMBER
ARL-TR-6157

9. SPONSORING/MONITORING AGENCY NAME(S) AND ADDRESS(ES)

10. SPONSOR/MONITOR'S ACRONYM(S)

11. SPONSOR/MONITOR'S REPORT NUMBER(S)

12. DISTRIBUTION/AVAILABILITY STATEMENT
Approved for public release; distribution unlimited.

13. SUPPLEMENTARY NOTES

14. ABSTRACT
This report describes the measurement of the two-photon absorption coefficient of gallium phosphide (GaP) at 9.4 fsec as measured with a unique *Z*-scan measurement system designed to support the shortest possible laser pulses. The *Z*-scan system is designed to minimize dispersion of the ultrashort laser pulse as it propagates so that the shortest possible pulse reaches the sample, as well support the entire 220-nm bandwidth of the pulse. Using the standard laboratory and analysis methods of Sheik-Bahae et al., we obtain a two-photon absorption coefficient, β, of GaP of 1.02 cm/GW at 800 nm, a value commensurate with measurements at performed at longer pulse widths. To the best of our knowledge, this is the first determination of the two-photon absorption coefficient of GaP below 10 fsec.

15. SUBJECT TERMS
Z-scan, two-photon absorption

16. SECURITY CLASSIFICATION OF:			17. LIMITATION OF ABSTRACT	18. NUMBER OF PAGES	19a. NAME OF RESPONSIBLE PERSON
a. REPORT	b. ABSTRACT	c. THIS PAGE			Robert C. Hoffman
Unclassified	Unclassified	Unclassified	UU	24	19b. TELEPHONE NUMBER (*Include area code*) (301) 394-0815

Contents

List of Figures

List of Tables

1. Introduction

We report the construction of a dispersion-minimized *Z*-scan setup to measure third-order optical nonlinearities in thin samples of semiconductors and thin films of organic materials on substrates. The use of dispersive media in the optical path has been eliminated, except for 1 mm of fused quartz used in the beam splitters required for beam characterization. In this report, we measure the two-photon absorption coefficient of <100> oriented undoped crystalline gallium phosphide (GaP). So far as we know, this is the first determination of the two-photon absorption coefficient of GaP below 10 fsec.

2. Theory: Z-scan Technique

The Z-scan method (*1*, *2*) was developed as a simple way to determine nonlinear changes in refractive index and absorption using a single light beam, and it can be used for solids and liquids. The technique involves translating a sample (on the "z" axis) through a tightly focused beam. Many materials will exhibit an intensity dependent absorption or refraction, $n(I) = n_0 + n_2 I$, where n_0 is the linear index of refraction, n_2 is the nonlinear index of refraction, and I is the incident intensity. If the sample exhibits nonlinear refraction or absorption, the transmitted intensity will change based upon the nonlinearity. A schematic of the *Z*-scan experiment is shown in figure 1. A thin sample with a n_2<0 when translated through the beam focus will collimate the transmitted beam to an extent, leading to an increase in transmission provided there is an aperture in front of the detector (closed aperture *Z*-scan). As the sample passes through the focus, the transmitted intensity returns to normal, and then past the focus, the light will be defocused to an extent, leading to a decrease in the transmitted intensity. If n_2>0, then the situation will be reversed. In the current application, we seek to determine the two-photon absorption coefficient, and generally an open aperture *Z*-scan is used, so that all that is observed is the nonlinear absorption. The transmitted intensity $\Delta T(z)$ is of the general form:

$$\Delta T(z) \approx \frac{q_0}{[1+Z^2/Z_0^2]} \tag{1}$$

where $q_0 = \beta I_0 L_{eff}$ and Z is the sample position and Z_0 is the position of focus. L_{eff} is calculated using $L_{eff} = (1 - e^{-\alpha l})/\alpha$, where α is the linear absorption and l is the sample length. Here β denotes the third-order nonlinear absorption coefficient, which for ultrafast nonlinear absorption is equal to the two-photon absorption coefficient. I_0 is the irradiance upon the sample and for a beam of Gaussian transverse profile and hyperbolic secant temporal profile the irradiance is

$$I_0 = \frac{2E}{\pi \omega_0^2 \tau} \tag{2}$$

where E is the pulse energy (J), $\omega_0$is the $1/e^2$ spot size, and τ is the pulse duration as measured by the autocorrelator. ω_0 is calculated using $\omega_0 = 1.27\lambda f/2d$, where f is the focal length of the focusing element and d is the measured beam diameter. The Rayleigh range, the range over which the beam is considered to be focused, is $Z_R = \pi\omega_0^2/\lambda$. It is important that the sample be thinner than the Rayleigh range in order for the thin sample approximation to be used.

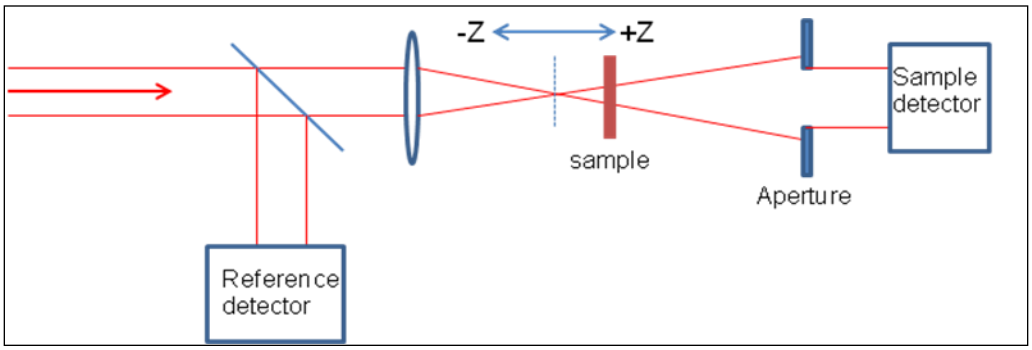

Figure 1. Schematic of a *Z*-scan experiment.

When calculating β (in units of cm/GW) using the expression $q_0 = \beta I_0 L_{eff}$, q_0 is obtained as a parameter from the *Z*-scan fit while the irradiance comes from equation 2. The Fresnel losses at the entrance face of the GaP sample must be accounted for, and for GaP, the loss is about 28%; the absorption from 700 to 920 nm is negligible (*3*). Due to the negligible absorption, L_{eff} in the equation for q_0 can be considered equal to L. While thermo-optic effects due to the high average power of titanium (Ti):sapphire lasers are important in liquids, these effects are negligible in semiconductors, and each pulse from the pulse train can be considered to be an independent measurement of the semiconductor sample (*4*, *5*).

3. Femtosecond Pulses

3.1 Generation of Ultrashort Pulses

A mode-locked femtosecond laser uses a broadband gain medium such as Ti:sapphire in which a "frequency comb" (figure 2) consisting of a large number of longitudinal modes (well over one million) that are oscillating with a fixed phase relationship with one another such that a pulse train is generated. The bandwidth of the pulses can be very large, greater than 200 nm in some cases, and even octave-spanning (*6*). The mode spacing ω_{M} is on the order of the repetition rate, i.e., 75 MHz, and this fixed phase relationship between adjacent longitudinal modes is very stable once the conditions are favorable for a pulse train to be established.

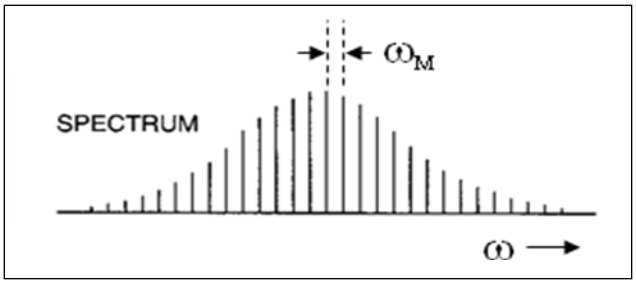

Figure 2. Frequency comb of a mode-locked laser.

An infinite train of pulses (figure 3) from a mode-locked laser can be written as (*7*)

$$E(t) = \boldsymbol{III}\left(\frac{t}{T}\right) * f(t) \tag{3}$$

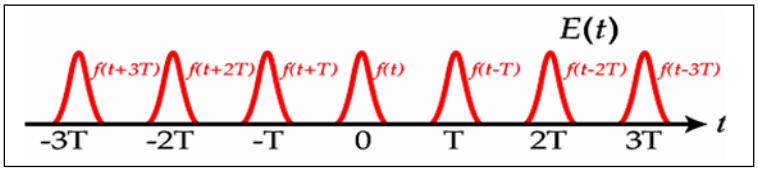

Figure 3. Pulse train from a mode-locked laser.

where ***III*** is a "fence" function or "Shah" function used to describe either the pulse train or the frequency comb, T is the time between pulses, $f(t)$ is the shape of each pulse, and $*$ denotes the convolution operation. Since the Convolution Theorem states that the convolution of two functions is the product of their Fourier transforms so we obtain (figure 4)

$$\tilde{E}(\omega) \propto \boldsymbol{III}\left(\frac{\omega t}{2\pi}\right) F(\omega) \tag{4}$$

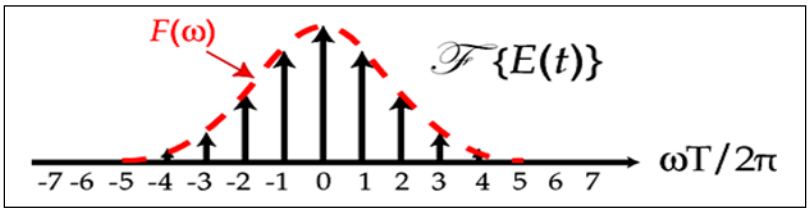

Figure 4. Frequency comb of a mode-locked laser.

This is assuming that the pulse train results from a single pulse oscillating within the cavity. The spacing between frequencies is $\Delta\omega = \frac{2\pi}{T}$, or alternatively, $\Delta\upsilon = 1/T$. Because the spectrum and the pulse shape are related by a Fourier transform, the shape of the spectrum has a profound impact on the shape of the pulse:

$$E(t) = \int_{-\infty}^{\infty} \tilde{E}(\omega) e^{2\pi i \omega t}\, d\omega \tag{5}$$

where *E*(t) is the electric field as a function of time. The spectrum is obtained by the Fourier inversion theorem:

$$\tilde{E}(\omega) = \int_{-\infty}^{\infty} E(t) e^{-2\pi i \omega t} dt \quad (6)$$

As a result of this property, any change in the spectrum will result in undesirable changes in the pulse shape. A perfect *sech*^{2} pulse will have a spectrum that is also a *sech*^{2} shape, since *sech*^{2} is its own Fourier transform. Thus, it is critical that all optical components that reflect or transmit the pulse not alter the spectrum in any way.

While pulsed lasers often emit pulses that are Gaussian with respect to their temporal intensity, mode-locked femtosecond lasers emit pulses that are hyperbolic secant with respect to their temporal electric field:

$$E(t) = E_0 sech\left(t/\tau\right) \quad (7)$$

where E(t) is the electric field with respect to time and τ is the pulse width at full width half-maximum (FWHM). It follows then that the intensity observed experimentally with respect to time is

$$I(t) = I_0 sech^2\left(t/\tau\right) \quad (8)$$

Generally, femtosecond *sech*^{2} pulses exist only as such within the laser cavity. Once the pulses exit the laser, they are subject to a variety of spatio-temporal distortions; dispersion being chief among them. However, most experimenters treat the pulses as *sech*^{2} pulses once they propagate outside the laser cavity; this is valid so long as there is no dispersion.

3.2 Dispersion in Transparent Media

A femtosecond laser pulse, when travelling through any transparent medium of refractive index $n(\omega)$ and length L, will experience a spectral phase shift due to the chromatic dispersion of the medium (*8*). The chromatic dispersion of an optical medium is basically the frequency dependence of the phase velocity with which light propagates in the medium. Because of the very large bandwidth of the pulse, one defines dispersion of second and higher orders via the Taylor expansion of the phase ϕ as a function of the angular frequency ω, around some center frequency ω_0 (note that ω_0 in this case denotes frequency and not spot size, as in section 2):

$$\phi(\omega) = \phi(\omega_0) + \phi'(\omega_0)(\omega - \omega_0) + \frac{1}{2}\phi''(\omega_0)(\omega - \omega_0)^2 + \frac{1}{6}\phi'''(\omega_0)(\omega - \omega_0)^3 + \ldots \quad (9)$$

where $\phi(\omega) = n(\omega)kL = k(\omega)L$ and $k_o = \omega_o/v_p$. The first derivative

$$\frac{d\phi}{d\omega} = \frac{d(k(\omega)L)}{d\omega} = L\left(\frac{d\omega}{dk}\right)^{-1} = \frac{L}{v_g} = T_g \quad (10)$$

results in the group delay T_g, which describes the delay of the peak of the envelope of the pulse. For convenience, the refractive index as a function of frequency $n(\omega)$ can be expressed in terms of wavelength λ:

$$T_g = \frac{d\phi}{d\omega} = \frac{L}{c}\left(n + \omega\frac{dn}{d\omega}\right) = \frac{L}{c}\left(n - \lambda\frac{dn}{d\lambda}\right) \quad (11)$$

As the beam propagates, the "quasimonochromatic" waves move at different speeds through the material and the pulse begins to broaden. This second-order dispersion is called the group delay dispersion (GDD):

$$GDD = \frac{d^2\phi}{d\omega^2} = \frac{L}{c}\left(2\frac{dn}{d\omega} + \omega\frac{d^2n}{d\omega^2}\right) = \frac{\lambda^3}{2\pi c^2}\frac{d^2n}{d\lambda^2} \quad (12)$$

Dispersion is often considered up to the third order (TOD):

$$TOD = \frac{d^3\phi}{d\omega^3} = \frac{L}{c}\left(3\frac{d^2n}{d\omega^2} + \omega\frac{d^3n}{d\omega^3}\right) = \frac{-\lambda^4 L}{4\pi^2 c^3}\left(3\frac{d^2n}{d\lambda^2} + \lambda\frac{d^3n}{d\lambda^3}\right) \quad (13)$$

The units of GDD and TOD are in units of fs^2/rad and fs^3/rad^2, respectively, but usually the units are simplified to fs^2 and fs^3. Typical values for T_g, GDD, and TOD for 1 mm of fused quartz are 4900 fs, 40 fs^2, and 28 fs^3, respectively, at 800 nm. Values for a high index glass such as SF10 by contrast are 5800 fs, 143 fs^2, and 97 fs^3, respectively, at 800 nm. This indicates that fused quartz should be used whenever possible within the optical system. Other materials such as calcium fluoride (CaF_2) and beryllium oxide (BeO) have less dispersion but are not commonly used.

3.3 Laboratory Methods for Measuring Ultrashort Pulses

Two common methods for analyzing ultrashort pulses are interferometric autocorrelation (*9*) and frequency resolved optical gating (FROG) (*10*). Both are based upon the Michelson interferometer, and in both cases, a second-order nonlinearity (second harmonic generation [SHG]) is required to achieve the autocorrelation. In the case of the interferometric autocorrelation, the pulse to be analyzed is split, and the time-delayed replica of the pulse is recombined collinearly within a SHG crystal at the output of the Michelson interferometer to provide the autocorrelation signal:

$$\boldsymbol{I_M(\tau) = \int_{-\infty}^{\infty} \left|\left(E(t) + E(t-\tau)\right)^2\right|^2 dt} \quad (14)$$

The interferometric autocorrelation provides some information about the dispersion or "chirp" within the pulse. The output is in the form of an interferogram with signal strength on the vertical axis and delay on the horizontal axis. There are four terms associated with the interferogram: a DC term equal to 1; a term that oscillates at ω with an amplitude of 4:1 relative to the DC term; a term that oscillates at 2ω with an amplitude of 1:1 relative to the DC term; and the envelope of the interferogram, which is the intensity autocorrelation, which has an amplitude of 3:1 relative to the DC term. The combined interferogram should ideally exhibit an 8:1 from peak to the DC value.

A more complete measurement of the phase within the pulse is accomplished with FROG, which essentially takes the output of the Michelson interferometer in the interferometric autocorrelation case and spectrally resolves it:

$$I_{FROG}^{SHG}(\omega,\tau) = \left|\int_{-\infty}^{\infty}\left(E(t) + E(t-\tau)\right)e^{-i\omega t}dt\right|^2 \quad (15)$$

With this method, the pulse can be graphically displayed with time along the horizontal axis and frequency (or wavelength) on the vertical axis. In this way, it is easy to quantify the phase and chirp of the pulse in an unambiguous manner. There is a directional ambiguity because a second-order nonlinearity is used to detect the autocorrelation, but this can be removed, if needed, by using a third-order nonlinearity, Most of the time, determining the magnitude of the chirp is most important, not whether the chirp goes up or down with frequency. Regardless of the method used, we determined that it was important to measure both the direct output of the laser and what is downstream in the optical system using one of these techniques in order to understand as much as possible the true nature of the pulses entering the sample.

4. Experiment and Discussion

4.1 Pulse Characterization

The instrumentation for measuring the interferometric autocorrelation is in immediate proximity to the exit port of the femtosecond laser in order to monitor the average output power, spectrum, and autocorrelation of the femtosecond pulses on a continuous basis. The results from the interferometric autocorrelation measurements (spectrum and autocorrelation) are shown below.

The spectrum (figure 5), as measured shows a 220 nm full width. It is important that the full width be considered, since all oscillating longitudinal modes contribute to the pulse train. There is a noticeable hump near 840 nm that will limit how short the pulses can be, since the spectrum deviates from the ideal $sech^2$ pulse shape. The spectrum will change slightly from day-to-day as the local environment within the laser changes.

The interferometric autocorrelation is shown in figure 6 and indicates the presence of some third-order dispersion, as indicated by the slight "humps" on either side of the main interferogram. It exhibits a peak-to-DC ratio of 6.7:1, which is not the ideal 8:1, but is the maximum available for this autocorrelator. The pulse width is obtained from the interferogram by taking the center wavelength of the spectrum (780 nm) and by the relation $\Delta\tau = \lambda_0/c$ calculating the fringe spacing, which equals 2.60 fsec in this case. By counting and interpolating between the number of fringes N the pulse duration (FWHM) is then $\tau_{pulse} = N\Delta\tau/D$, where D is a deconvolution factor. For a $sech^2$ pulse, D = 1.897 (*12*). For these parameters, a value of the FWHM pulse width of 9.4 fsec is obtained.

In this *Z*-scan experiment, not only is dispersion control important, but understanding what is impinging upon the sample is important as well. We placed a Swamp Optics 8-20 USB FROG (GRENOUILLE) unit in the optical path at approximately the same distance the sample (~1 m) is from the output port of the laser. The spectrum as measured is shown in figure 7. The bandwidth is in excess of 200 nm in this measurement and the phase is flat, indicating a well-compressed pulse. We should note that at 9.4 fsec the pulses we are measuring are near the limits of what the instrument can accommodate.

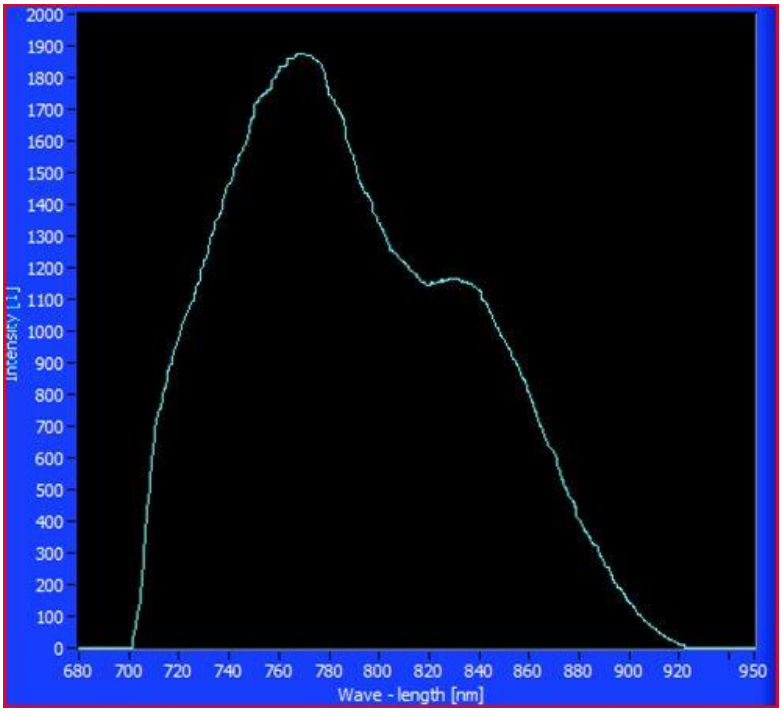

Figure 5. Spectrum of a FemtoLasers mode-locked Ti:sapphire laser.

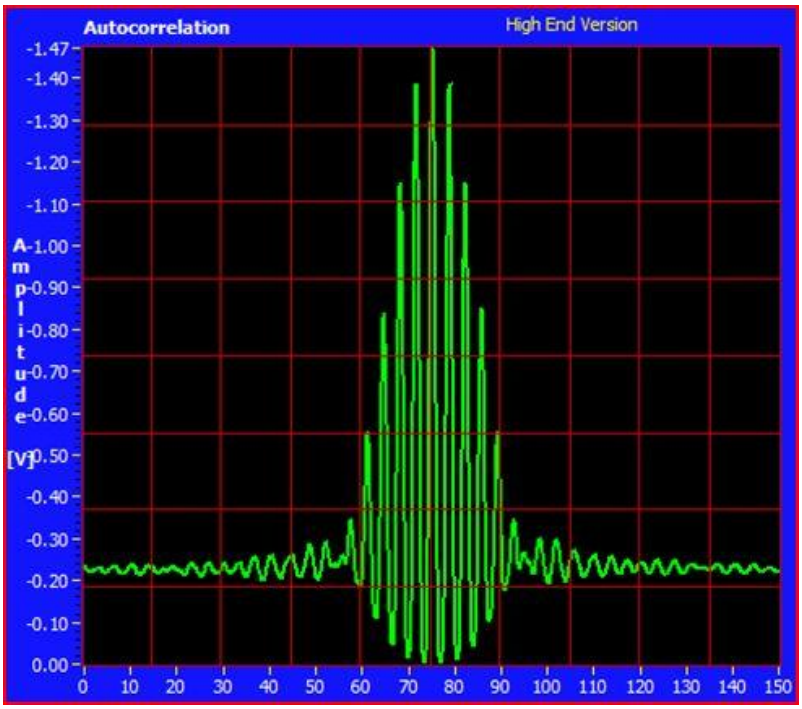

Figure 6. Interferometric autocorrelation of a FemtoLasers mode-locked Ti:sapphire laser.

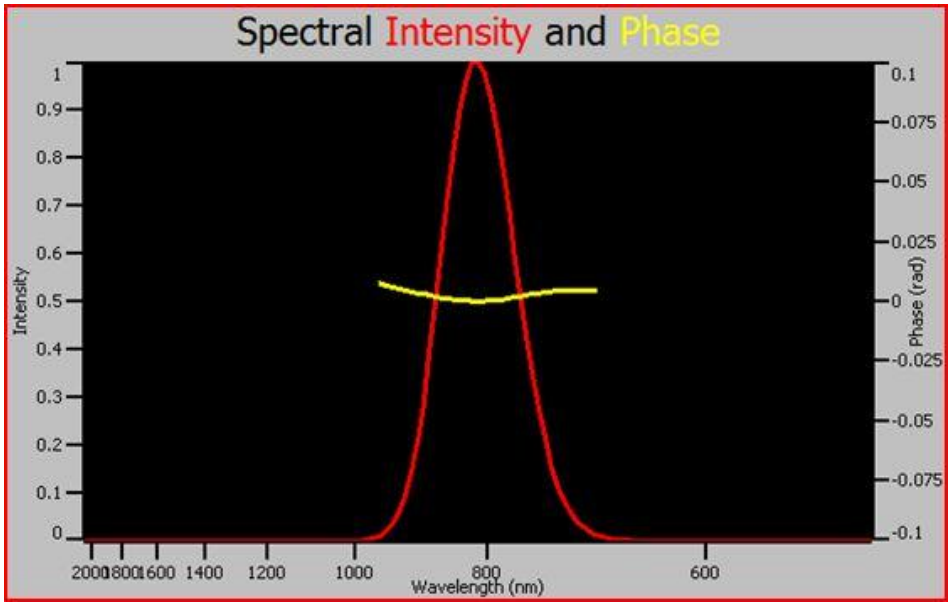

Figure 7. Spectral intensity and phase of FemtoLasers mode-locked Ti:sapphire laser as measured by FROG at ~1 m from output port.

The retrieved FROG spectrogram trace, shown in figure 8, indicates little "chirp" or dispersion in the pulse. This is indicated by the lack of any appreciable expansion of the spectrogram to the left or right, relative to the spectral width. The sensitivity of the detector did not allow the lower intensity levels of the spectrogram to be displayed, hence the discrepancy between the spectral

intensity measurement and the bandwidth displayed by the FROG trace. The pulse width as measured is 9.21 fsec with a FWHM time-bandwidth product of 0.45, indicating the presence of some residual third-order phase distortion. This third-order phase distortion is also visible as a slight pear-shape imparted to the FROG trace. The results from the interferometric autocorrelation and the FROG measurement are similar at 9.4 and 9.21 fsec, respectively. We are reasonably confident that what enters the front face of the sample is a sub-10 fsec pulse train.

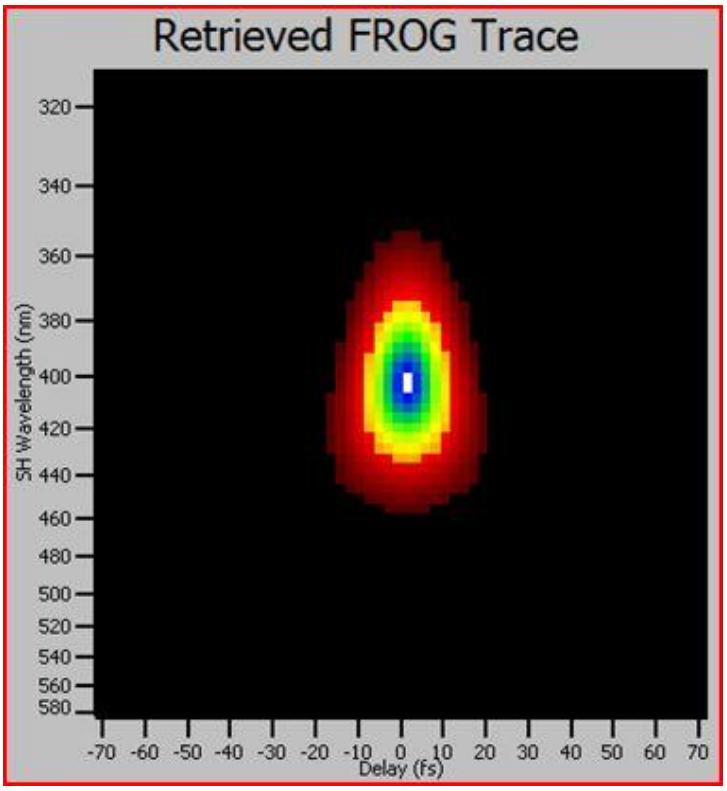

Figure 8. FROG Spectrogram of FemtoLasers mode-locked Ti:sapphire laser as measured by FROG at ~1 m from output port.

4.2 Beam Profile

To measure the beam profile, we used a Data Ray, Inc., WinCamD digital profiling camera, coupled with Data Ray profiling software. The results of the data capture are shown in figure 9. The beam profile, shown in figure 9, has an ellipticity of 0.93, but the average value of the beam diameter of 1.537 mm was used in all the calculations. The actual values are 1.743 and 1.427 mm for the vertical and horizontal profiles, respectively. The horizontal beam fit shown in figure 10 has a Gaussian fit of 87% and the vertical beam fit shown in figure 11 has a Gaussian fit of 96%.

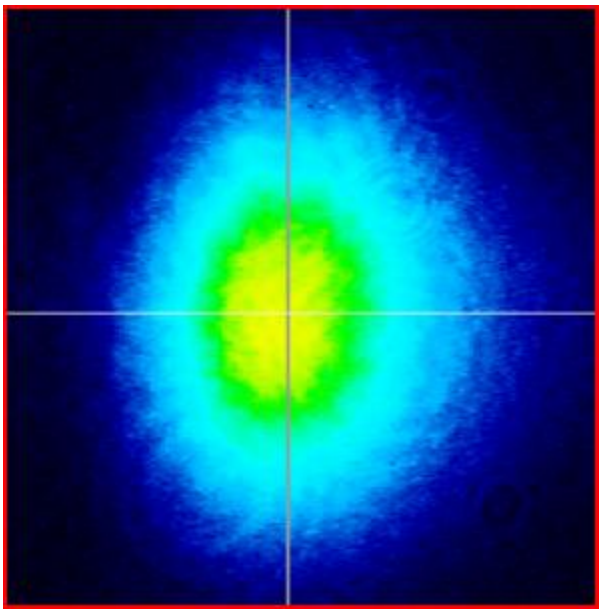

Figure 9. Beam profile of FemtoLasers mode-locked Ti:sapphire laser.

We consider the beam to be Gaussian for the purposes of this experiment. The features we observe, i.e., beam ellipticity, etc., are common in continuous wave (CW)-pumped Ti:sapphire lasers. Spatial filtering would no doubt improve the profile somewhat, but any conventional spatial filtering technique using refractive elements would introduce unwanted dispersion. There is usually some astigmatism in CW-pumped Ti:sapphire lasers and this could be corrected by introducing a 2-mm undoped sapphire element that is at Brewster's angle, but in the opposite sense of the gain crystal to null out the astigmatism. This would necessitate focusing the beam into the sapphire compensating element, necessitating the use of undesirable dispersion-introducing refractive elements. A Spiricon beam tap was used in conjunction with a ND = 1.0 filter to reduce the average power to a level that would not saturate the WinCamD detector. The beam profile and the fits (figures 10 and 11) are generally consistent from day-to-day.

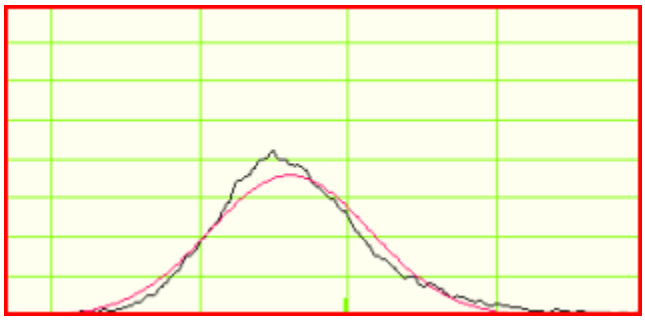

Figure 10. Horizontal beam fit; Gaussian fit = 87%.

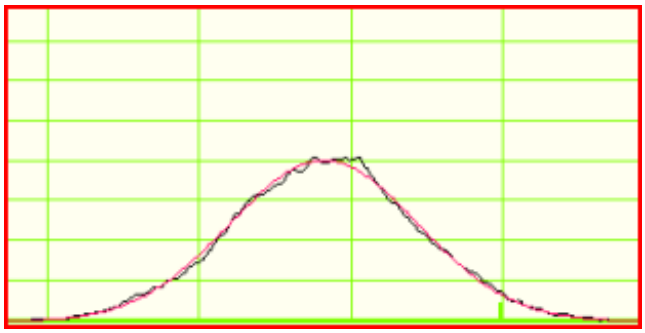

Figure 11. Vertical beam fit; Gaussian fit = 96%.

4.3 Z-scan Measurement

The *Z*-scan measurements were performed using the system shown in figure 12. The laser is a FemtoLasers Synergy Pro Ti:sapphire laser emitting a train of pulses at 75 MHz with an average power of 550 mW. The pulse experiences some dispersion in the cavity, and this is compensated by the use of five bounces off a pair of dispersion controlled mirrors. Immediately upon exiting, the laser the pulses are characterized first by the autocorrelator, which uses a first surface refection off of a 0.5-mm-thick fused quartz beamsplitter. The beam then is analyzed by the near-infrared (NIR) spectrometer, which also uses a first surface refection off of a second 0.5-mm-thick fused quartz beamsplitter. The beam then impinges upon a first-surface removable mirror. The surfaces of all mirrors are either protected aluminum or ultra-wideband dielectric mirrors designed to support the full 220-nm bandwidth of the pulse. The removable mirror can direct the beam either to the FROG (GENOUILLE) unit or to the 50-mm focal-length off-axis parabolic first-surface mirror, (FemtoLasers part # OA027). The off-axis parabolic mirror focuses the pulses on the sample, where they are collected by the sample detector, an Ophir Laserstar CW detector. A Newport ESP300 Universal Motion Controller/Driver drives the sample along the *z*-axis. In order not to introduce any more dispersive elements than needed, the first experiments are being performed with no reference leg, and the laser appears to be stable enough to perform the measurement in this way. A close-up view of the 50-mm focal-length off-axis parabolic first-surface mirror and the GaP sample are shown in figure 13. The pulses enter from bottom center of the photo, are reflected by the off-axis parabolic mirror, and enter the sample from the right. In this way, we introduce no dispersive effects during focusing of the sample (*13*), a feat simply not possible with any kind of refractive element. This ensures as much as possible that a sub-10 fsec pulse enters the front face of the sample.

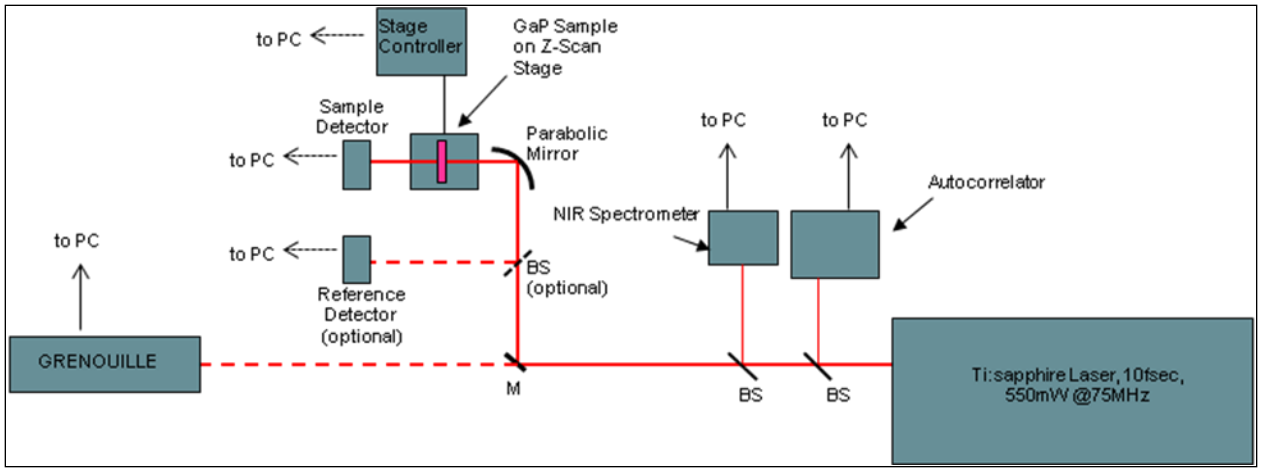

Figure 12. Dispersion-minimized sub-10 fsec *Z*-scan optical layout.

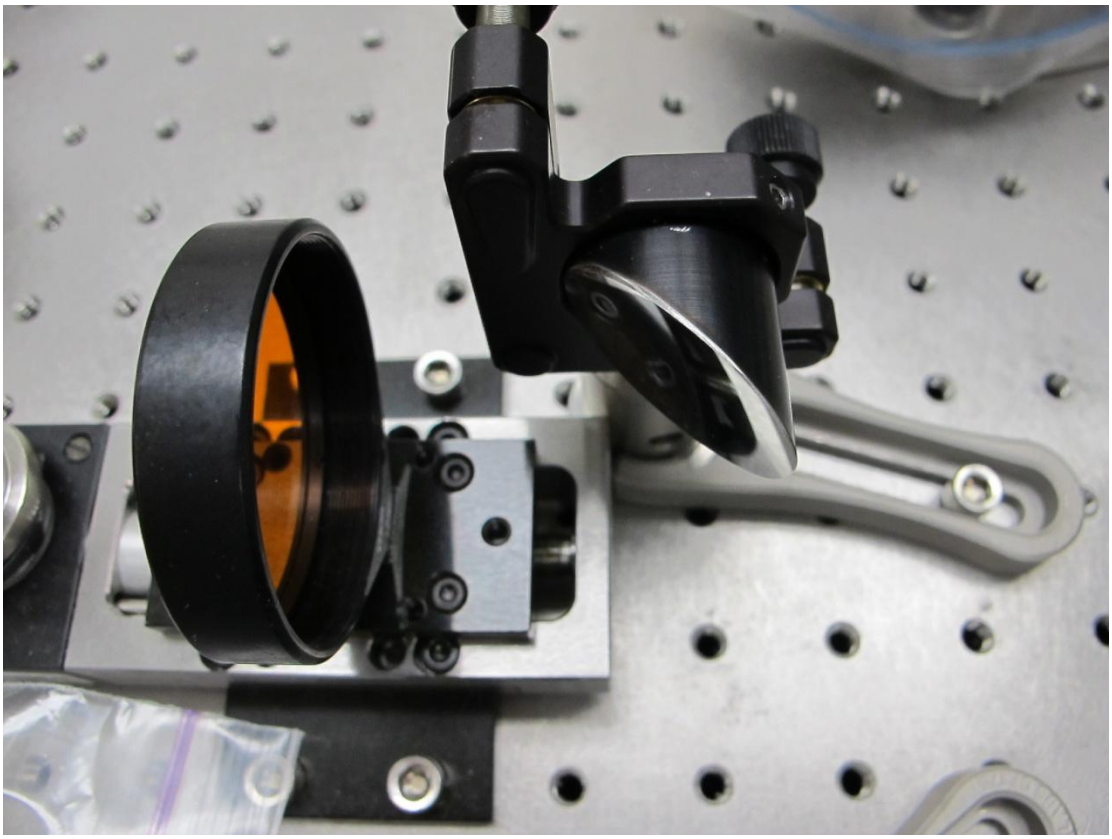

Figure 13. A close up view of the 50 mm focal-length off-axis parabolic first-surface mirror and the GaP sample.

Figure 14 shows the *Z*-scan data obtained using a 0.5-mm-thick undoped <100> oriented GaP crystal wafer obtained from MTI Corporation. We measured the incident energy at the entrance face of the sample to be 903 pJ. The step size was 0.5 mm. The experiment was performed to gather data out to ± 10 mm to ensure a proper fit to determine q_0. The fit on both sides of the

minimum is good, indicating good power stability of the laser during the scan. A filter (ND = 1.0) was placed in front of the detector to prevent saturation.

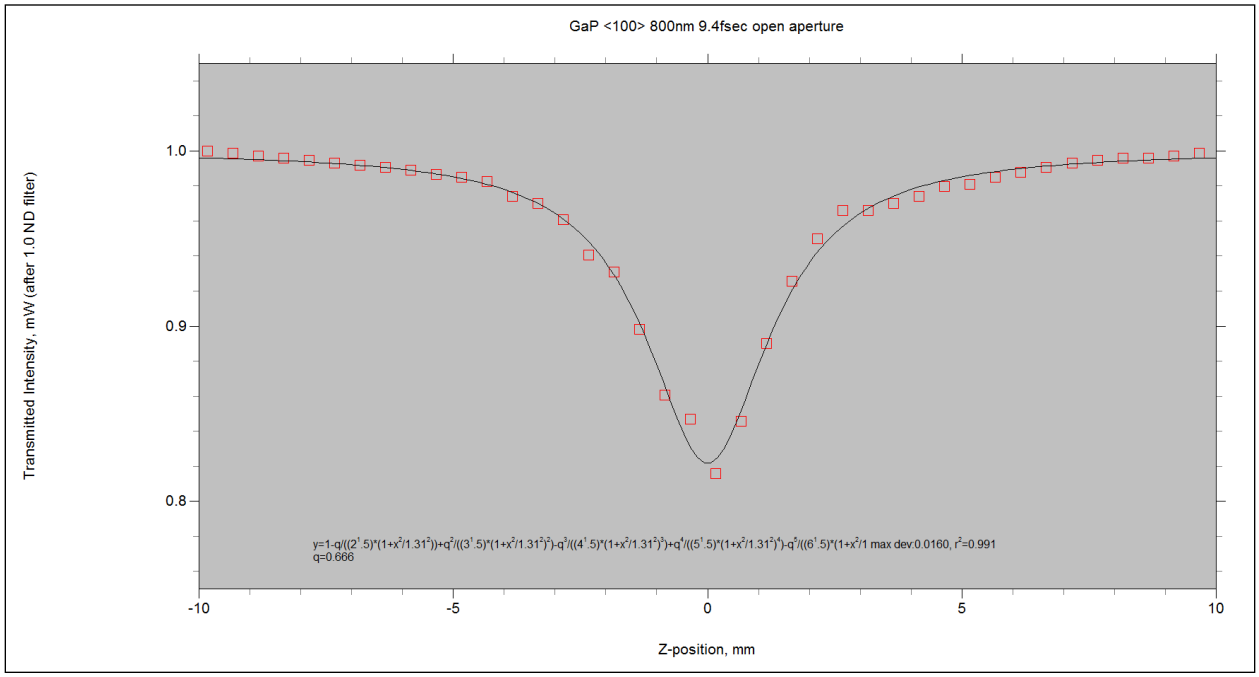

Figure 14. Open aperture *Z*-scan data for undoped <100> oriented GaP.

From reference 2, the transmission of the laser through the sample in an open aperture *Z*-scan configuration can be expressed as

$$T(z) = \sum_{m=0}^{\infty} \frac{[-q_0(z)]^m}{(m+1)^{\frac{3}{2}}} \tag{16}$$

We performed a linear least squares fit to the data using the first six terms of the summation fitting for both the Rayleigh range, Z_R, and for q_0. We calculated a Rayleigh range value of 1.07 mm based on the beam size before the off-axis parabolic mirror, but the data fit much better to a Rayleigh range of 1.31 mm (corresponding to a spot size of 18.3 μm). We attribute the difference to aberrations in the original laser beam that have yet to be quantified, and that our beam is not collimated before reflecting off of the parabolic mirror. Since the calculated Rayleigh range is 1.31 mm, which is more than twice as thick as the sample tested, this ensures that the thin sample approximation is valid.

A summary of all the parameters used to calculate the two-photon absorption coefficient, β, is shown in table 1. The value of β we calculate for undoped <100> GaP is 1.02 cm/GW. There is scant data in the literature for β measurements of GaP, particularly in the femtosecond regime. However, Bechtel *et al*. measured a value of 0.2 cm/GW using a picosecond 1064-nm laser (*14*). The value we measured is commensurate with the previous value, and we expect the value of β to be relatively constant from the psec regime to the sub 10 fsec regime. This is due to the fact

the two-photon absorption is a sub-fsec process and is considered instantaneous for both time regimes.

Table 1. Experimental parameters used to calculate two-photon absorption coefficient of GaP.

Parameter	Equation	Value
Spot size ω_0, (from *Z*-scan fit)	$\omega_0 = 1.27\lambda f/2d$	1.83 x 10^{-3} cm
Rayleigh range, Z_R	$Z_R = \pi\,{\omega_0}^2/\lambda$	0.107 cm
Irradiance, I_0	$I_0 = \dfrac{2E}{\pi\omega_0^2\,\tau}$	22.5 GW/cm^2
q_0	From *Z*-scan fit	0.666
Sample thickness, L_{eff}	measured	0.05 cm
Front Face Reflection, %	(from ref. 3)	28%
TPA coefficient, β	$\beta = q_0/I_0L_{eff}$	**1.02 cm/GW**

5. Future Improvements to Z-scan System

In the future, we plane to address some of the limitations and sources of error in the present procedure. One of the most important is to measure the spot size and beam profile at focus to examine what spatial distortions, if any, occur at focus and correct for them if possible. The ellipticity of the beam may be compensated for using the method in Mian et al. (*15*), if needed. Another source of error occurs when translating the sample in the *z*-direction that often results in the translation of the focused spot on the sample in the *x*- and *y*-directions, resulting in different volumes of material being sampled. An alignment procedure performed by a *z*-translation with the beam waist passing consistently through a pinhole will eliminate this problem, if it exists. In addition, including a reference arm can eliminate any tilt of the wings of the *Z*-scan due to the power drop that sometimes occurs in CW-pumped Ti:sapphire lasers as the cavity adjusts to the thermal equilibrium. Also, many of the functions in this experiment were done manually, but will be automated. These include translation of the sample stage and data collection. Perhaps the most intriguing from a scientific point of view will be the addition of a NIR spectrometer behind the sample to monitor the changes in the 220-nm spectrum that enters the sample. We expect significant changes to the spectrum as it passes through focus, with certain portions of the spectrum being absorbed preferentially. As we gain experience with the technique and make improvements, we will refine the value of the two-photon absorption coefficient for GaP and begin measuring the two-photon absorption coefficient of other semiconductors such as cadmium sulfide (CdS) and zinc selenide (ZnSe). We will also begin measuring the two-photon absorption coefficient for organic thin-film materials deposited on various substrates.

6. References

1. Sheik-Bahae, M.; Said, A. A.; Van Stryland, E. W. High-sensitivity, Single-beam n_2 Measurements. *Optics Letters* **1989**, *14* (17).

2. Sheik-Bahae, M.; Said, A. A.; Van Stryland, E. W.; Wei, T-H; Hagan, D. J. Sensitive Measurement of Optical Nonlinearities Using a Single Beam. *IEEE Journal of Quantum Electronics* **1990**, *26* (4).

3. Aspnes D. E.; Studna, A. A. Dielectric Functions and Optical Parameters of Si, Ge, GaP, GaAs, GaSb, InP, InAs, and InSb from 1.5 to 6.0 eV. *Phys. Rev.* **1983**, *B27* (2), 985-1009.

4. Li, H. P.; Kam, C. H.; Lam, Y. L.; Zhou, F.; Ji, W. Nonlinear Refraction of Undoped and Fe-doped $KTiOAsO_4$ Crystals in the Femtosecond Regime. *Appl. Phys.* **2000**, *B 70*, 385.

5. Krauss, Todd D.; Wise, Frank W. Femtosecond Measurement of Nonlinear Absorption and Refraction in CdS, ZnSe, and ZnS. *Appl. Phys. Lett*. **1994**, *65* (14).

6. Matos, L.; Kleppner, D.; Kuzucu, O.; Schibli, T. R.; Kim, J.; Ippen, E. P.; Kaertner, F. X. Direct Frequency Comb Generation from an Octave-spanning, Prismless Ti:Sapphire Laser. *Optics Letters* **2004**, *29* (14).

7. Trebino, R. Convolution and Autocorrelation, Georgia Tech Department of Physics Lectures.

8. Wollenhaupt, M.; Assion, A.; Baumert, T. Femtosecond Laser Pulses: Linear Properties, Manipulation, Generation and Measurement. *Springer Handbook of Lasers and Optics* In Springer Handbook of Lasers and Optics, 2007, pp. 937–983.

9. Diels, J.; Fontaine, J.; McMichael, I.; Simoni, F. Control and Measurement of Ultrashort Pulse Shapes (In Amplitude and Phase) with Femtosecond Accuracy. *Applied Optics, 24*, 1270.

10. Trebino, R.; DeLong, K. W.; Fittinghoff, D. N.; Sweetser, J. N.; Krumbügel, M. A.; Richman, B. A. Measuring Ultrashort Laser Pulses in the Time-frequency Domain Using Frequency-resolved Optical Gating. *Rev. Sci. Instrum*. **1997**, *68*, 3277–3295.

11. Konoplev, O.; Meyerhofer, D. Cancellation of B-Integral Accumulation for CPA Lasers. *IEEE Journal of Selected Topics Quantum Electronics* **March/April 1998**, *4* (2).

12. Femtometer Dispersion Minimized Autocorrelator user manual, Femtolasers Produktions GmbH, 2007, p. 13

13. Bor, Z. Distortion of Femtosecond Laser Pulses in Lenses and Lens Systems. *Journal of Modern Optics* **1988**, *35* (12), 1907.

14. Bechtel, J. H.; Smith, W. L. Two-photon Absorption in Semiconductors with Picosecond Laser Pulses. *Phys. Rev. B* **1976**, *13*, 3515.

15. Mian, S. M.; Taheri, B.; Wickstead, J. P. Effects of Beam Ellipticity on Z-scan Measurements. *JOSA B* **1996**, *13* (5).

1 (PDF only) DEFENSE TECHNICAL INFORMATION CTR
DTIC OCA
8725 JOHN J KINGMAN RD
STE 0944
FORT BELVOIR VA 22060-6218

1 DIRECTOR
US ARMY RESEARCH LAB
IMAL HRA
2800 POWDER MILL RD
ADELPHI MD 20783-1197

1 DIRECTOR
US ARMY RESEARCH LAB
RDRL CIO LL
2800 POWDER MILL RD
ADELPHI MD 20783-1197

1 DIRECTOR
US ARMY RESEARCH LAB
RDRL CIO LT
2800 POWDER MILL RD
ADELPHI MD 20783-1197

3 US ARMY RESEARCH LAB
ATTN RDRL SEE M
R C HOFFMAN BLDG 207 Z3D-46-15
2800 POWDER MILL RD
ADELPHI MD 20783-1197

1 US ARMY RESEARCH LAB
ATTN RDRL SEE M
A G MOTT BLDG 207 Z3D-46-20
2800 POWDER MILL RD
ADELPHI MD 20783-1197

INTENTIONALLY LEFT BLANK.